Nanostructure to Microstructure Self-Assembly of Aliphatic Polyurethanes: The Effect on Mechanical Properties

ARTICLE *in* THE JOURNAL OF PHYSICAL CHEMISTRY B · APRIL 2010

Impact Factor: 3.3 · DOI: 10.1021/jp100599u · Source: PubMed

3 AUTHORS, INCLUDING:

Vinod K Aswal
Bhabha Atomic Research Centre
392 PUBLICATIONS **4,906** CITATIONS
SEE PROFILE

Pralay Maiti
Indian Institute of Technology (Banaras Hi…
102 PUBLICATIONS **3,641** CITATIONS
SEE PROFILE

Nanostructure to Microstructure Self-Assembly of Aliphatic Polyurethanes: The Effect on Mechanical Properties

Abhinay Mishra,[†] Vinod K. Aswal,[‡] and Pralay Maiti*,[†]

School of Materials Science and Technology, Institute of Technology, Banaras Hindu University, Varanasi 221 005, India and Solid State Physics Division, Bhabha Atomic Research Centre, Trombay, Mumbai 400 085, India

Received: January 21, 2010; Revised Manuscript Received: March 18, 2010

We report the step by step self-assembly from nanostructure to microstructure (bottom-up approach through X-ray diffraction (1.6 nm), small angle neutron scattering (SANS) (11.6 nm), atomic force microscopy (70 nm smaller crystallite from enlarged image and 450 nm greater crystallites), and polarizing optical microscope (2 μm)) of aliphatic polyurethanes (PU) in contrast to aromatic polyurethanes depending on hard segment content (HSC). Polyurethanes of 10 to 80% HSC have been synthesized by using appropriate amount of polyol and chain extender. The effect of self-assembled patterns on mechanical properties both in solid and liquid state has been established exhibiting structure−property relationship of supramolecular polyurethanes. The crystallinity enhances but the degradation temperature decreases with increasing HSC. The characteristic length (measure of gap between lamellar crystallites), as revealed from SANS, gradually decreases with increasing HSC suggesting compactness of the crystallites through extensive hydrogen bonding. The Young's modulus increases with increasing HSC with a percolation threshold of hard segment (50%) while the toughness improves up to 30% HSC followed by gradual decrease in presence of bigger crystallites which promote brittle fracture. The origin of self-assembly in aliphatic PUs has been demonstrated through electronic structure calculations to form a loop structure with minimum intermolecular distance (2.2 Å) while that distance is quite large in aromatic polyurethanes (4.6 Å) that cannot form hydrogen bonds. The unique splintering of domain structure and its subsequent reformation under dynamic shear experiment has been established.

Introduction

Synthetic polymers like polyurethanes having the properties of biocompatibility and biodegradability are a special class of materials and are being used in biomedical applications, high-performance elastomeric product, biomaterials, durable coating, and shape memory materials.[1–9] Polyurethanes are most versatile polymer constituted by hard and soft segments. Thermodynamic incompatibility between hard and soft segments is responsible for unparalleled combinations of strength, stiffness, and toughness by altering the composition of the constituents. The explicit feature of these hard and soft segments drives the polymer system into two phase morphology in which hydrogen-bonded, crystalline hard microdomains form amid the rubbery soft domains.[10–14] Depending on the specific segmental composition and the interactions between soft−soft and hard−soft, the hard microdomains can form fibrillar, globular, cylindrical, or lamellar structures within a continuous soft matrix or form an interconnected hard-domain network. The flexibility of urethane chemistry enables the structure/shape of the domains to control various properties of the polyurethane.[15,16]

Cooper and co-workers[17–19] have defined the presence and behavior of the hydrogen bonds on mechanical properties of polyurethanes. Velankar et al.[20] have reported the phase mixing through small-angle X-ray scattering (SAXS) and rheological measurements. Further, temperature-resolved SAXS experiments have demonstrated gradual microphase mixing of the microphase-separated materials with increasing temperature.[21] Koberstein and co-workers[22,23] have demonstrated temperature-induced changes in the hard microdomain structure. The temperatures corresponding to the microcrystalline melting and microphase disordered endotherms increase with both the hard segment content and annealing temperature. The morphological changes that accompany these alterations in thermal properties have been studied by simultaneous SAXS and differential scanning calorimetry (DSC) measurements.[24–26] A more detailed discussion of the peak temperature trends and the consequences of this behavior in terms of structure−property relations have been presented therein. Klinedinst et al.[27] have worked on the polyurethaneurea based on hydrogenated diphenyl methane diisocyanate and hexamethylene diisocyanate in addition to either ethylene diamine or 2-methyl-1,5-diaminopentane as the chain extender. The morphologies of these materials have developed microphase separation with wide service windows as measured using SAXS and dynamic mechanical analyzer (DMA). In addition to the broad temperature insensitive plateau, they displayed a unique, near linear, Hookean-like stress−strain response until fracture at very high levels of strain in excess of 900% in some cases. Direct visual evidence of the microphase-separated morphology has also been reported by using atomic force microscopy (AFM) for polyurethaneurea-based materials. Recently Vaia and co-workers[28] have reported transient microstructure of low hard segment thermoplastic polyurethane under uniaxial deformation. Further, they have concluded from X-ray experiments that the neat low hard segment polyurethane system shows a transient morphology at low strains, dominated by soft segments crystallites, involving the coexistence of two independent crystalline phases. The subsequent mechanical properties are associated with these soft segment crystallites, which

* To whom correspondence should be addressed. E-mail: pmaiti.mst@itbhu.ac.in.
[†] Banaras Hindu University.
[‡] Bhabha Atomic Research Centre.

10.1021/jp100599u
Published on Web 04/02/2010

differentiates low hard segment thermoplastic polyurethane (TPUs) from conventionally used TPUs with greater amount of hard segments.

Syntheses and structural organization of mostly aromatic segmented polyurethanes have been worked out in the literature,[29–34] except a few on aliphatic segmented polyurethane,[35–38] because of their improved mechanical properties. The hard-segment zones are linked up through hydrogen bonds that are formed by reaction of diisocyanate and chain extender, thereby, raising enough scope for domain formation in hard segment zone depending on the chemistry involved. The microstructure and phase morphology[17,39–42] of mostly aromatic polyurethanes have been demonstrated, but so far there is no report of nanostructural configuration leading to the formation of microstructure up to optical range and structure−property correlation thereof with molecular modeling.

In this work, we have outlined the self-assembly of aliphatic polyurethanes from nanostructure to microstructure (bottom-up approach) in contrast to aromatic-based polyurethanes. The effect of self-assembled patterns on mechanical properties have been delineated both in solid and liquid state exhibiting structure−property relationship of supramolecular polyurethanes. The origin of self-assembly has been demonstrated through electronic structure calculations that illustrates that aliphatic polyurethanes form a loop structure with minimum intermolecular distance while that distance is quite large for aromatic polyurethanes. The thermal properties have been elucidated by using thermogravimetric analysis (TGA), differential thermal analysis (DTA), and DSC. The detailed crystallite structure is described through small-angle neutron scattering (SANS) techniques.

Experimental Section

Materials. Poly(tetramethylene glycol) (PTMG) (Terathane, Sigma Aldrich), number average molecular weight (M_n) 2900 g/mol, 1,6-hexamethylene diisocyanate (HMDI) and 1,4-butanediol (BD) (Merck, Germany) were used as received. The catalyst dibutyltin dilaurate and solvent dimethyl formamide (DMF) were purchased from Himedia and Loba Chemie, respectively.

Synthesis. The polyurethanes (PU) were synthesized in two steps. First step is commonly referred to the prepolymer formation from polyol and excess diisocyanate to produce an isocyanate-terminated molecule. The prepolymer generally has a low molecular weight, but can be as high as 15 000−20 000 and is either a viscous liquid or low-melting solid. Subsequent reaction of this prepolymer with a chain extender (butane diol) constitutes the second step, which produces a multiblock copolymer of the segmented polyurethanes. By varying the diol/chain extender and diisocyanate, PU with different hard segment contents (HSC) were synthesized from 10 to 80% HSC using the above method. In the first stage, polyol (PTMG) and diisocyanate (HMDI) were mixed at a constant temperature of 70 °C for 4 h to form an isocyanate-terminated prepolymer in a closed reaction vessel. In the second stage, the prepolymer was treated with 1,4-butanediol as chain extender in presence of catalyst (dibutyltin dilaurate) with rapid stirring at the same temperature for 24 h in an inert atmosphere. The polymer was extracted by pouring the solution in deionized water and dried in vacuum at reduced pressure at 60 °C for 48 h. The molecular weights as measured by gel permeation chromatography (GPC) for all PUs are 35 000−40 000. The hard segment content was varied by using different amount of polyol, diisocyanate, and chain extender. The numbers after PU indicate the HSC content in percentage.

Characterization. Proton NMR spectra were recorded on a JEOL AL 300 spectrometer using d_6-DMF as solvent. Each spectrum was recorded after the sample was equilibrated in the magnetic field at least for 10 min. The chemical shifts are reported in parts per million relative to tetramethylsilane. Infrared spectra were recorded on a Thermo Nicolet 5700 Fourier transform IR (FTIR) of thin solid polymer film taking 100 scans with the resolution of 4 cm^{-1}.

X-ray Diffraction (XRD). X-ray diffraction was performed using Bruker AXS D8 Advance wide-angle X-ray diffractometer with a graphite monochromator using CuKα source with a wavelength of 0.154 nm. The generator was operated at 40 kV and 20 mA. The thin sheet of the samples was placed on a glass sample holder at room temperature and were scanned at diffraction angle 2θ from 1° to 40° at the scanning rate of 1° min^{-1} for detecting interplanar distance less than 4 nm.

Small-Angle Neutron Scattering (SANS). SANS experiments were performed on the spectrometer at the Dhruva reactor at Bhabha Atomic Research Centre, Mumbai, India. The data were collected in the scattering vector ($\mathbf{q}$) range of 0.17 $nm^{-1} \leq \mathbf{q} \leq 3.5$ nm^{-1}. The scattering from the samples were corrected for the solvent and background contributions. The lower $\mathbf{q}$ range was fitted separately with Debye-Bueche and other models. The characteristics length (Λ_c) was calculated using the equation $\Lambda_c = 2\pi/\mathbf{q}_m$, where $\mathbf{q}_m$ is the scattering vector $\mathbf{q}$ corresponding to the peak position of the shoulder in the scattering pattern. The temperature was kept constant at 30 °C during every measurement.

Differential Scanning Calorimetry (DSC). The degree of crystallinity, melting, crystallization temperatures and heats of fusion of the PUs were determined via DSC using Mettler 832 over a temperature range of −20 to 250 °C at a scan rate of 10 °C min^{-1}. The samples were heated at the scan rate of 10 °C/min. The peak temperature and enthalpy of fusion were measured from the endotherms using a computer attached with the instrument. After the first melting, the samples were cooled down at a constant rate of 10 °C/min to find the crystallization temperature and heat of crystallization in a similar fashion. The peak temperature and enthalpy of fusion were measured from the second run. The DSC was calibrated with indium before use.

Morphological Investigation. The morphology of the thin film of PU was investigated by using scanning electron microscope (SEM), AFM, and polarizing optical microscope (POM). The surface morphology of pure polyurethane flakes was examined with a Hitachi H-7100 scanning electron microscope operated at an accelerating voltage of 15 kV for detecting submicrometer object. All the samples were gold coated by means of a sputtering apparatus under vacuum before observation. A NT-MDT multimode atomic force microscope, Russia, controlled by Solver scanning probe was used for surface morphology study. Tapping mode was used with the tip mounted on 100 μm long single beam cantilever with resonant frequency in the range of 240−255 kHz, and corresponding spring constant of 11.5 N/m. Thin film of ∼100 μm was used for AFM studies after suitably processing them through melt pressing to notice the submicrometer to micrometer objects. The morphology of thin film (∼30 μm) in optical range was examined using a POM (Nikon) after quenching the samples at room temperature on a Mettler hot stage for detecting micrometer size object.

Microinjection. For tensile testing, standardized specimens were prepared via microinjection using microinjector (model

FD-1, Fly Tech Engineering). The various HSC content samples were microinjected at a barrel temperature of T_m + 20 °C and mold temperature of 25 °C with a pressure of 100 bar.

Mechanical Properties. Tensile tests were performed with the injection-molded samples using an Instron 3369 tensile tester at a strain rate of 5 mm min^{-1} at room temperature. Several samples were tested to obtain good error estimates.

Dynamic Mechanical Characterization. Frequency dependence of oscillatory shear moduli in the liquid state was measured, using dynamic frequency sweep tests, on Rheologica (model: Nova) using parallel plate geometry (25 mm) at various temperatures between ~(T_m + 10 °C) to ~(T_m + 80 °C) keeping the strain amplitude of 0.05 to maintain linear response of the sample. The measured angular frequency ω for oscillatory shear experiment was kept in the range from 0.5 to 300 rad/s. The storage moduli and complex viscosities were measured as a function of angular frequency for aliphatic/aromatic PU with various HSC content. Oscillation control experiment was conducted at fixed frequency as a function of time. The frequencies were chosen as per the dip region in frequency sweep experiment.

Steady Shear Viscosity. Steady shear viscosity in the liquid state was measured using, constant shear rate test, on a Reologica model Nova using cone−plate geometry (25 mm) at T_m + 20 °C at various shear rate ($\dot{\gamma}$ = 0.001 to 0.1 s^{-1}).

Modeling. To understand the polymer chain conformation, molecular modeling has been carried out through energy minimization program to interpret intermolecular interactions involved in polyurethane with aliphatic and aromatic part in polymer chain. We have initially optimized a part of polyurethane chain at least with one diisocyanate, polyol, and chain extender unit in it. A semiempirical AM1 method, as implicated in Chem3D Ultra 7.0, was used to obtain the optimized geometries. Those optimized structures were then used to understand the hydrogen bonded interactions, believed to be the governing factor for cluster formation between the >C═O groups of one molecules with the >N−H group of another chain of polyurethane. We have modeled polyurethane as a truncated chain consisting of minimum 32 carbon, 4 nitrogen, and 11 oxygen atoms.

Results and Discussion

NMR and FTIR Spectroscopy. The spectroscopic characterization on each polymer involved ^{1}H NMR and FTIR. Typical representative NMR spectra of polyurethanes are given in Figure 1a. The features of these spectra are in complete agreement with the respective component of the polymer chain.[31,43,44] The intensity of >N−H peak at 7 ppm gradually increases with hard segment content. Figure 1b shows the FTIR spectra of PUs with varying hard segment content. The peak at 3315 cm^{-1} corresponds to hydrogen-bonded N−H stretching and the peak intensity gradually increases with increasing hard segment content of PU.[32,35,40,45,46] The two peaks between 2950 and 2850 cm^{-1} corresponds to CH_2 asymmetric vibration present in soft segments and the intensity gradually decreases with increasing hard segment content which clearly indicates that the soft segment (−CH_2−CH_2) decreases with increasing HSC. The peak at 2355 cm^{-1} has been assigned to cyano band-stretching frequency in the urethane linkage and the intensity of the peak gradually increases with hard segment content which confirms that the number of HN−CO group increases with HSC content.[30,40,45,46] The other prominent peak at 1685 cm^{-1} has been assigned for carbonyl group of urethane present in hard segment.[14,35] Here also, the intensity of the peaks increases with HSC content. However, spectroscopic analyses exhibit the varying amount of hard segment in aliphatic-based PUs.

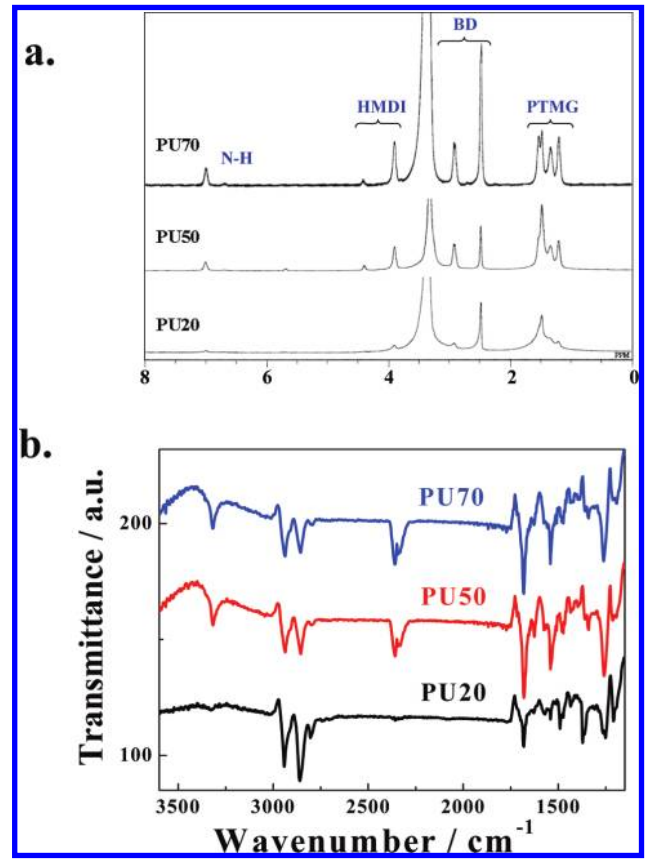

Figure 1. (a) NMR and (b) FTIR spectrum of HMDI−PTMG−BD-based polyurethane with different hard segment content as mentioned.

Crystallinity and Structure. Figure 2a shows the XRD patterns of PUs with different HSC. PU20 exhibits predominantly amorphous hallow while the crystalline peaks at 20.6, 22.2, and 23.8° appear for higher hard segment content PUs. The gradual enhancement of peak intensity indicates greater crystallinity for higher HSC PUs. The higher crystallinity is also recognized from DSC thermograms of PU samples (Figure 2b). Here again, PU20 is amorphous (no peak appears at higher temperature region) and the melting endotherm emerges starting from PU30. The heat of fusion as mentioned in the figure increases with increasing HSC. The melting temperature gradually increases with HSC of PU samples indicating ordered and thicker crystallites of high HSC PUs made of hydrogen bonded hard segments.[24,47,48] The double endotherms of the melting peak appear from the melt-recrystallization of PU.[26,49] The lower temperature endotherm at ~25 °C matches with the melting point of pure PTMG and the peak intensity gradually decreases with increasing HSC as PTMG content is getting lesser in high HSC PUs.

Small-Angle Neutron Scattering (SANS). To look inside the crystallite patterns, SANS[50−55] has been measured to examine the detail structure in the **q** range of 0.017 to 0.35 $Å^{-1}$. Figure 3a shows the SANS patterns of the various HSC PUs. Figure 3b represents the SANS pattern of PU80 with error bar. A distinct shoulder is evident in the middle portion of **q** which is also seen in other PUs. These peaks are indicative of a stacked lamellar pattern inside the crystallite. Interestingly, the peak position gradually shifted to higher **q** range with increasing HSC. The characteristic lengths, $\Lambda_c = 2\pi/\mathbf{q}_m$, are 16.2, 13.9, 12.4, and 11.6 nm for PU20, PU50, PU70 and PU80, respectively,

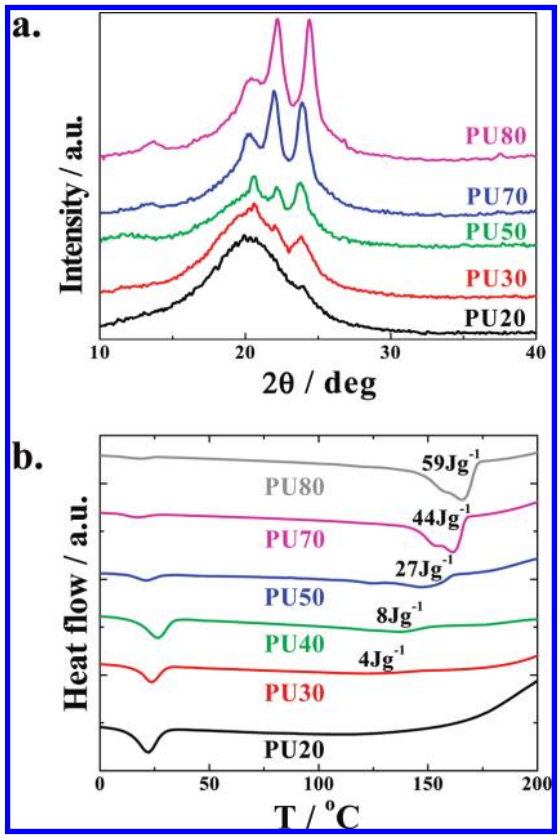

Figure 2. (a) Wide-angle X-ray diffraction of PUs with varying HSC content. (b) DSC thermograms of indicated PUs in the second run. The values in $J \cdot gm^{-1}$ indicate the heat of fusion of PUs.

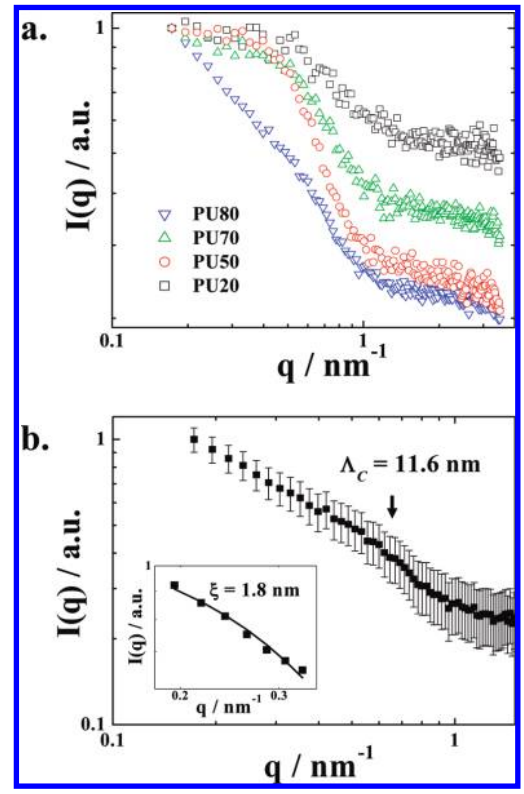

Figure 3. (a) Small-angle neutron scattering patterns; $I(\mathbf{q})$ vs $\mathbf{q}$ (wavevector) plot of indicated *PUs*. (b) SANS pattern of representative PU80 showing error bar. The down arrow indicates the peak position. Inset figure show the Debye-Buche fitting for low-$\mathbf{q}$ range.

where $\mathbf{q}_m$ is the wavevector corresponding to peak position. Hence, the gap between the lamella decreases with increasing HSC. The lower and higher $\mathbf{q}$ regions can be fitted with Debye-Bueche model (eq 1) to know the correlation length (ξ). One such fitting has been shown in the inset of Figure 3b. It is evident that the fittings are not so fine because of the presence of hump. However, the calculated ξ values are 0.9, 0.55, 0.6, and 1.7 nm for PU20, PU50, PU70, and PU80, respectively. The reciprocal of structure factor versus scattering vector has been plotted to check the validity of the other models as well. There is no ordered plateau at higher $\mathbf{q}$ range, which indicates that the experimental data do not fit the Ornstein−Zernike model (eq 2) while lower $\mathbf{q}$ range fits moderately with Debye-Bueche model.

$$I(\mathbf{q}) = \frac{I(o)}{(1 + \xi^2\mathbf{q}^2)^2} \quad (1)$$

$$I(\mathbf{q}) = \frac{I(o)}{1 + \xi^2\mathbf{q}^2} \quad (2)$$

However, it is evident from SANS experiment that the correlation length and the characteristics length have the same decreasing order with increasing HSC and the size the crystallites become greater for higher HSC PUs.

Thermal Properties. Figure 4a shows the TGA thermograms of PUs with varying HSC content. The degradation temperature decreases with increasing HSC and the values are 300°, 288° and 283 °C for PU20, PU50, and PU80, respectively. The degradation temperature was calculated corresponding to temperature where 5% weight loss occurred in the sample. The degradation patterns have drastically been changed with varying hard segment content. PU20 exhibit two stages of degradation while three stages of degradation are observed in higher HSC PUs which is distinctly observed in subsequent DTA endothermic peaks (Figure 4b). The hard segment part (urethane linkage) is more susceptible toward heat and degrades first.[49] Thus, the isolated crystallites, made of exclusively hard segments, degrade first followed by the scattered crystallites embedded in soft segment. Finally, the soft segment degrades at relatively higher temperature range. DTA signals indicate that the first degradation (~300 °C) of high hard segment content sample occurs at lower temperature as compared to low HSC PUs, and, further, soft segment degradation temperature shifts to higher side promoting sequence of degradation of different segments of polyurethane. The low-temperature peak at 175 °C for PU80 is due to the melting of the hard segment, and the absence of the same in lower HSC PUs is explained from the meager amount of hard segment to get the DTA signal response.

Self Assembly. With the increase of hard segment content, the domain structure becomes prominent and organized for aliphatic polyurethanes as observed in polarizing optical microscope (Figure 5a). The more ordered cylindrical domains, within the above domain in optical micrographs, have been observed in AFM topographs in tapping-mode with same order of hard segment content (Figure 5b). The alternate black and white strip as observed in POM and AFM images suggest the segmentization of the hard and soft part of polyurethane. The black strip is the crystalline zone while the white region is mostly amorphous as evident from the enlarged part of the AFM image for PU20. Inside each black region there are several thinner black zones arising out of the different crystallites (shown in enlarged AFM images). On the contrary, the white zone has no such crystallite further suggesting segmentization

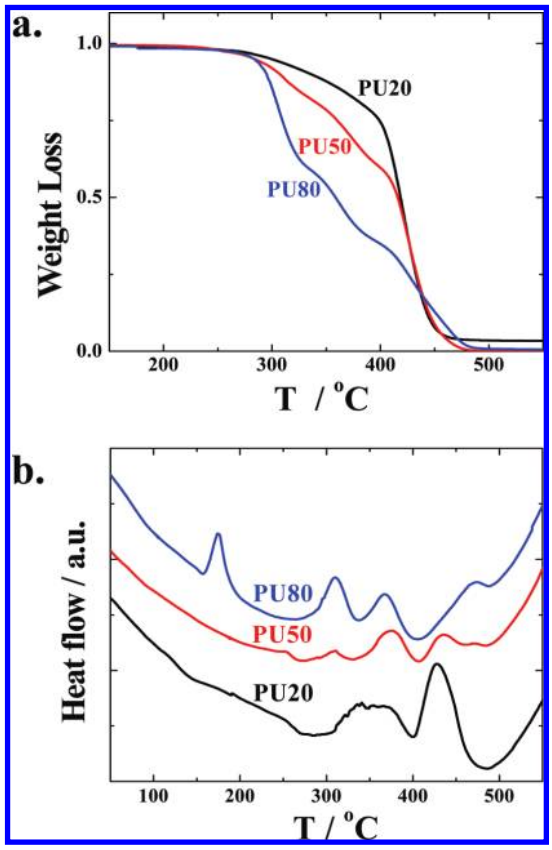

Figure 4. (a) Thermogravimetry conducted in air at a heating rate of 10 °C/min. (b) The corresponding DTA signal.

of the hydrogen-bonded hard segments. This segmentization has not occurred either in commercial or synthesized aromatic polyurethanes (Supporting Information Figure S1) and has been manifested in the form of circular spot in MDI-based PUs.[39,56,57] Furthermore, the development of the XRD peaks at $2\theta \sim 6^o$, corresponding to the d-spacing of 1.6 nm, with increasing hard segment content indicates a nanostructure within the cylindrical domain (Figure 5c). The bottom-up approach is evident where molecular planes/nanostructure, exhibited by XRD peak, assembled to form a domain, observed in AFM, which further accumulated into microstructure/clusters discernible in optical images. Small-angle neutron scattering patterns of aliphatic PUs exhibit a shoulder, corresponding to the characteristic length of $\Lambda_c \sim 11-16$ nm, clearly suggest a greater assembly of molecular planes as compared to nanostructure appeared in XRD patterns (1.6 nm). Nearly, 7−10 molecular planes depending on HSC accumulate further to form a greater assembly emerged in the form of shoulder in SANS patterns. The microclusters as observed in SEM surface morphology also support the self-assembly of domain which systematically grows with increasing HSC content in aliphatic PUs (Figure 6). Surprisingly, polyurethanes containing aromatic diisocyanate or aromatic chain extender, the nanostructure and auxiliary self-assembly is missing (Supporting Information Figure S2). Moderately strong secondary forces, for example, hydrogen bonding is supposed to be operating between molecules causing interlocking of the molecules/domains while the difficulty of formation of *H*-bonding in presence of bulky aromatic groups restrict the building of greater domain structure of PU containing aromatic diisocyanates or chain extenders. However, the formation of nanostructure and subsequent self-assembly favors the creation of domain or microclusters in aliphatic diisocyanate and domain extended polyurethane have been demonstrated through XRD (1.6 nm), SANS (11.6 nm), AFM (70 nm smaller crystallite from enlarged image, and 450 nm greater crystallites), and POM (2 μm) in sequence and the schematic bottom-up approach has been shown in the Scheme 1 both for aliphatic and aromatic PUs.

Mechanical Properties. The mechanical response (stress−strain curves) in universal testing machine has been plotted in Figure 7a. The Young's modulus increases gradually with increasing HSC while the elongation at break reduces. The values of modulus and toughness (area under the stress−strain curve) have been shown in Figure 7b as a function of HSC. The modulus enhances slowly up to 50% HSC and after that there is an abrupt change in modulus that further increases with HSC. The crystallite usually reinforces the polymer and larger crystallites in greater HSC PUs facilitate increasing modulus of PUs. The networking through hydrogen bonding in higher HSC PUs is extensive, as evident from the higher crystallinity in XRD and DSC thermograms, causing an abrupt increase in modulus after 50% HSC. On the other hand, toughness increases up to 30% HSC followed by gradual decrease with increasing HSC. The ductility of PU samples decreases as the crystallinity increases. Hence, the greater crystallinity reduces the toughness of PUs as the chances of brittle fracture are high enough in presence of bigger crystallites in higher HSC PUs.

Structural Changes under Dynamic Force. Steady-state measurements have shown the Young's modulus in the linear region. The storage and loss moduli are accessible through dynamic measurement. The networking due to the self-assembly of domains may have impact on mechanical properties as compared to domain free or smaller domain dimension PUs. The storage modulus, $G'(\omega)$, measured at $T_m + 20$ °C, increases gradually[20] with increasing HSC content over a wide range of angular frequency ω (Figure 8a). Interestingly, the modulus exhibits a plunge at specific range of ω and further increases with increasing frequency. Interestingly, the dip has been shifted systematically toward higher frequency for greater HSC PUs indicating the splintering of network followed by its reformation depending on the strength of assembly (superior for higher HSC PUs). To look inside the breakage of the structure with frequency, controlled oscillation experiments have been conducted at constant frequency (Figure 8b) for representative PU20. The storage modulus increases with time as usual at 25 rad·s^{-1} frequency (just before the onset of the dip) while $G'(\omega)$ decreases with time in the dip zone (40−50 rad·s^{-1}) and remain constant at high frequency (200 rad·s^{-1}, after the frequency range of dip) suggesting that the self-assembled structure breaks at particular frequency range depending on the strength of association and subsequently reform at higher frequency exhibiting reversible nature of the structure formation. Another possibility may be the microdomains undergo orientation and alignment at some critical frequency. Temporarily, the modulus may reduce during the alignment process. As the aligned domains form additional hydrogen bonds due to favorable energetic conformation, the storage modulus increases rather fast at higher frequency (after the dip). The temperature-dependence frequency sweep test indicates that the breakage/alignment takes place at lower frequency measured at higher temperature (Figure 8c) further supports the above discussion. The melt rheology results support the formation of extensive networking at higher HSC content. On the contrary, TDI/MDI-based aromatic PU shows both the $G'(\omega)$ and $\eta^*(\omega)$-like homopolymer melts (Supporting Information Figure S3) with lowering in value of initial slope (∼1.1), but, the slope is much higher than that of HMDI-based aliphatic PU (∼0.3), suggesting

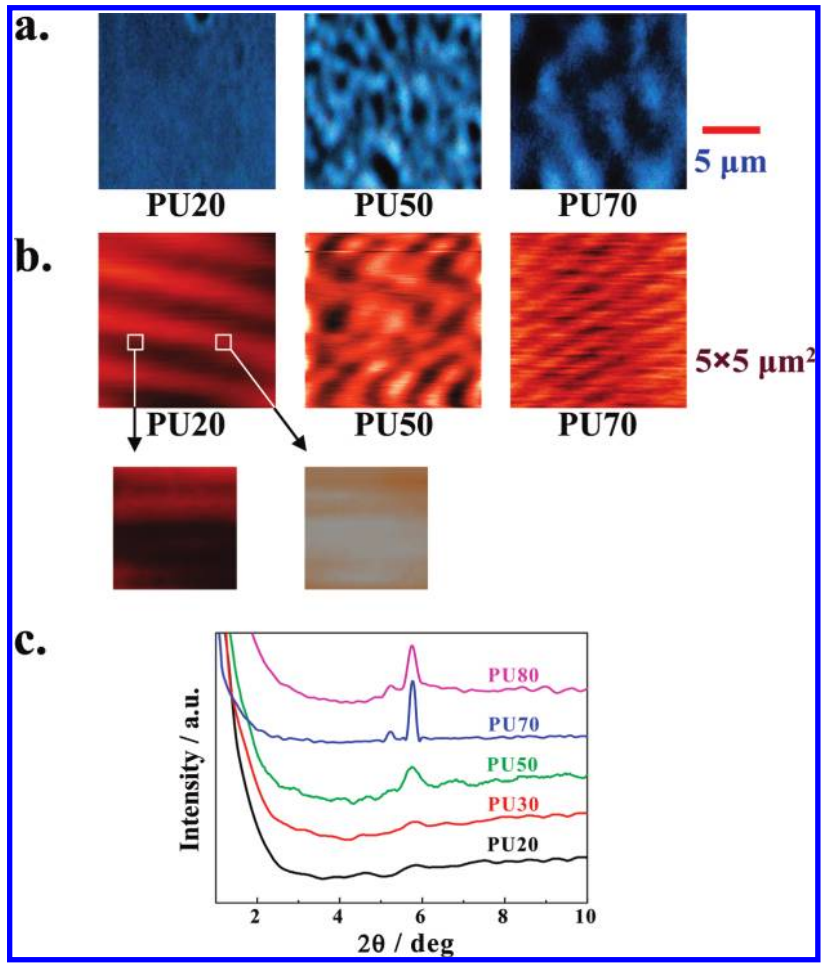

Figure 5. The self-assembled microstructure from nanostructure of aliphatic polyurethanes with hard segment content. (a) Optical images of aliphatic PUs showing gradual increase of cluster size with HSC. (b) AFM micrographs for various aliphatic PU which exhibit particular pattern with change in HSC. The enlarge part show further smaller crystallites within a bigger crystallite (left part) while the white part is amorphous (right part). (c) The X-ray diffraction patterns for indicated HSC content showing nanostructures. The *Y*-axes have been shifted for the sake of clarity. The numbers after PU indicate the hard segment content in percentage.

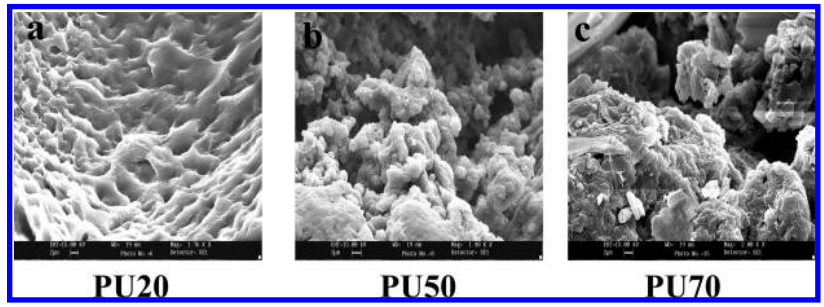

Figure 6. Scanning electron micrographs of polyurethanes with different hard segment content PU showing amorphous nature for low HSC content sample while crystalline clusters are evident for high HSC sample with a gradual change over from amorphous to crystalline morphology which also supports the XRD and DSC data.

only trivial interlocking of molecules causing very small cluster dimension as observed in POM and AFM morphology (Supporting Information Figure S2). Complementary proof of structure formation is obtained from gradual increase of viscosity in steady shear against the fall off the same for lower HSC content aliphatic PU as well as aromatic-based polyurethanes (Figure 8d). Hence, the mechanical properties improve a lot with increasing HSC content and the fascinating mechanical response due to the supramolecular structure/cluster formation through self-assembly have been revealed.

Molecular Modeling and Cluster Formation. To understand the reason of ordered self-assembly in aliphatic PU and not shaping the same for aromatic PU, the conformation of molecules in its minimized energy state have been construed by using semiempirical AM1 (electronic structure calculations) method. The lowest energy of a double strand of HMDI−BD-based (aliphatic) polyurethane take the shape of a loop with the minimum hydrogen-bonded distance between >C═O and H−N < group approaches to 2.2 Å (Figure 9, left portion). On the other hand, the lowest energy conformation of a strand of TDI−BD-based aromatic polyurethane chain is parallel to each other with the shortest distance between the above pair is 4.6 Å (Supporting Information Figure S4, left portion), more than twice the value of aliphatic PUs. Here, we preferred to choose a double strand to show the type of intermolecular forces operating between them. However, a close loop conformation

SCHEME 1: The Schematics of How the Nanostructure Transform into Microstructure through Self-Assembly in Aliphatic (Top) and Aromatic (Down) Polyurethane[a]

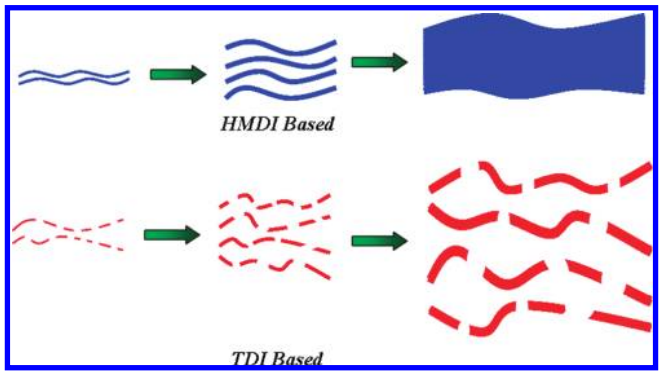

[a] The extreme right schemes show the large band structure in aliphatic PU while a fringed structure in aromatic PU (as observed in optical microscope). The middle one is exhibited in AFM morphology with moderate thick cylindrical domain in aliphatic PU and no pattern is observed for aromatic PU. The left schemes show the nanostructure only in aliphatic PU (as observed in XRD peaks). Although the thickening of layers occurs in aromatic PU, it does not lead to the formation of a band structure like aliphatic PU. However, the scheme can explain the development from nanostructure to microstructure (bottom-up approach) experimentally observed morphology both in aliphatic and aromatic PUs.

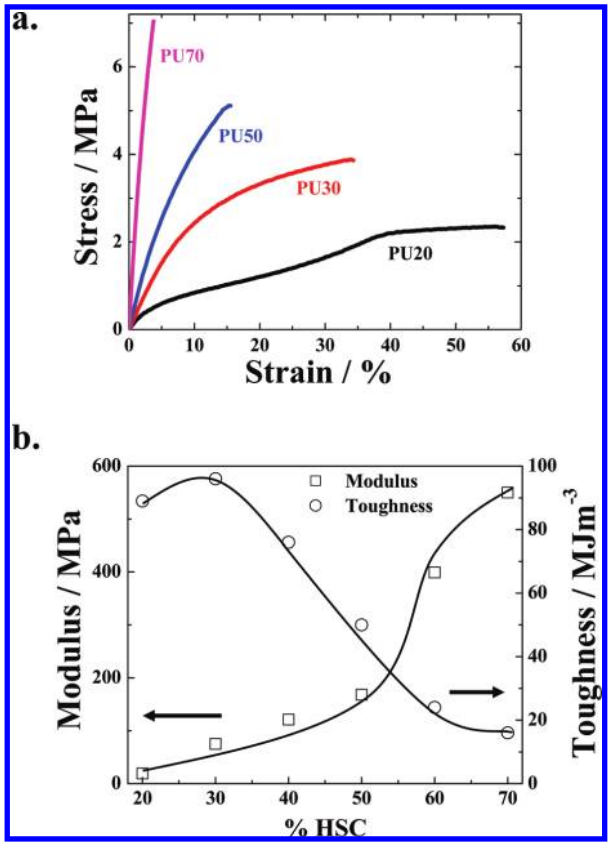

Figure 7. (a) Representative engineering stress−strain curves of polyurethanes with indicated hard segment content. (b) The modulus and toughness values (as calculated from the area under the stress−strain curve) for PUs as a function of hard segment content.

has been anticipated for aliphatic polyurethane and an extended close loop has been shown in schematics at the right side of Figure 9 and thereby constitute a molecular sheet/plane through H-bonding that is the basis for constructing the nanostructure. On the other hand, the minimum distance between two

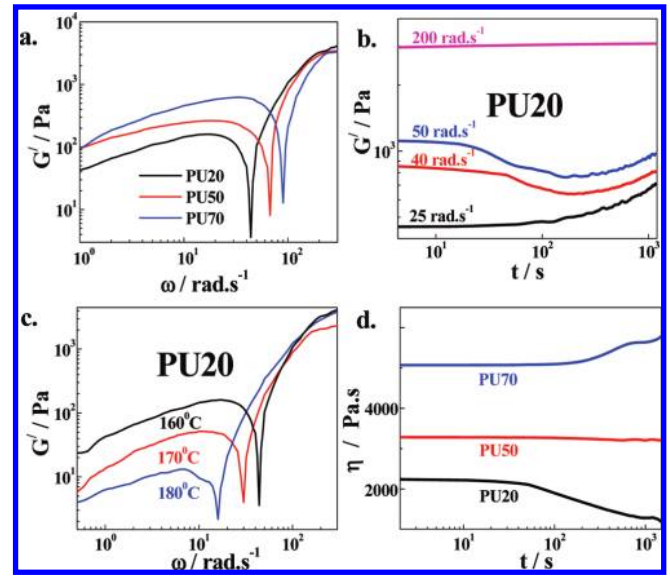

Figure 8. Mechanical responses of various polyurethanes in liquid state. (a) Storage modulus of HMDI−BD-based aliphatic PU with indicated hard segment content as a function of frequency. (b) Storage modulus as a function time in controlled oscillation experiments for fixed frequencies mentioned of aliphatic PU20 with indicated frequency, 25 rad·s^{-1} (before onset of dip), 40−50 rad·s^{-1} in the dip region and at 200 rad·s^{-1} (after the dip). (c) Storage modulus of PU20 from frequency sweep experiments at three representative temperatures, and (d) viscosity under steady shear condition at $\dot{\gamma} = 0.01$ s^{-1} for HMDI-based aliphatic PU with various HSC as mentioned.

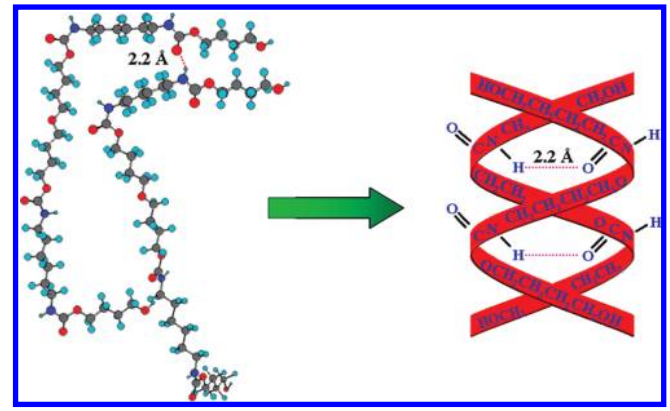

Figure 9. Molecular models of aliphatic polyurethane obtained from energy minimized electronic structure calculation from a part of chains in the left side showing the distance of hydrogen-bonded interaction sites leading to self-assembly in aliphatic diisocyanate and right portions indicate the schematic view of the organization from a bigger chain in aliphatic (HMDI)-based diisocyanate. A loop is apparent in the molecular modeling for aliphatic diisocyanate case.

molecules of the aromatic polyurethane is quite large and cannot construct any molecular plane. The XRD peak at ~6° originates from the molecular plane that also matches from the distance point of view from the molecular modeling. The larger intermolecular distances for aromatic polyurethane arise from the neighboring bulkier aryl groups associated with >C═O group present in the molecule. The molecular modeling predicts nicely the nature and extent of interaction through strong secondary forces and thereby acquires a particular conformation depending on the chemical constituents of polyurethanes. The other aromatic polyurethane also adopts the shape like TDI-based PU with shortest intermolecular distances of 4.2 and 5.8 Å for HMDI−biphenol and MDI−BD systems, respectively. Nonetheless, the planar molecular structure is evident for aliphatic PU only, while the rodlike structure is apparent for aromatic

PU due to H-bonding and its strength varies with intermolecular distances. The accessible >C═O and H−N< group in the other side of the loop (shown in the schematics of Figure 9) make them available for further self-assembly through H-bonding and help them grow giving rise to a domain/cluster patterns. Aromatic PU, with larger intermolecular distance, cannot form greater self-assembly. The limited nanophase separated hard segment domains have been found using AFM technique[39] for MDI-based PUs that cannot proceed further to create clusters in presence of bulky aromatic ring or, in other words, intense networking is missing. However, the better proximity of the aliphatic polyurethane chain can form strong network and ultimately generate large domain, responsible for improved properties.

Conclusion

Aliphatic polyurethanes containing 10 to 80% hard segment content have been synthesized. The degradation temperature decreases with increasing HSC as the urethane linkage in hard segment is more susceptible toward temperature. The sequential degradation has also been revealed from DTA responses. The Young's modulus gradually increases with increasing HSC while toughness increases up to 30% HSC followed by a gradual decrease. The larger crystallite acts as reinforcing agent for higher HSC PUs, which improves the modulus and much higher crystallinity, as observed from DSC and XRD studies, create them less ductile. The self-assembled network structure (bottom-up approach) with different length scale in aliphatic polyurethane has been demonstrated through XRD, SANS, AFM, and POM as opposed to aromatic polyurethanes. The cause of self-assembly pattern from nanostructure to microstructure through molecular modeling (electronic structure calculation) of aliphatic as well as aromatic polyurethane has been revealed to distinguish the chemical constituent dependence on clustering patterns leading to improved and controlled properties. The intermolecular distance is the lowest in aliphatic PUs (2.2 Å) while the gap increases in aromatic PUs (4.6 Å for TDI-based aromatic PU) depending on the ease of formation of hydrogen bonds in presence of aliphatic or aromatic groups. The splintering of network structure and its reformation at higher frequency has also been reported for the first time in pure polymer melts as evident from the dip in the storage modulus as a function of frequency. Further measurements at constant frequency for longer time and storage modulus at various temperatures in dynamic frequency tests also support the splintering and reformation of structure depending upon the strength of the assembly. The segmentization of soft and hard segment is evident from the AFM topographs. The detailed structure of the crystallites has been elucidated through SANS about the characteristic and correlation length to have deeper insight of the compactness of the molecular sheets in the crystallites.

Acknowledgment. The author (Abhinay Mishra) gratefully acknowledges the financial support from Council for Scientific and Industrial Research (CSIR), New Delhi in the form of fellowship (JRF and SRF). The authors acknowledge the research grant from Council for Scientific and Industrial Research Project No. 22(0399)/06/EMR-II. The authors also acknowledge the kind support of Dr. D. K. Avasthi, Mr. Pawan K. Kulriya and Dr. Biswajit Ray of IUAC, New Delhi and Chemistry Department, BHU for XRD and NMR measurements.

Supporting Information Available: Figures of AFM topograph of aromatic (TDI based) polyurethane, self-assembled microstructure and nanostructure of aromatic polyurethanes, frequency dependence storage modulus of aromatic (TDI based) polyurethane, and molecular model of aromatic polyurethane (TDI based) molecules. This material is available free of charge via the Internet at http://pubs.acs.org.

References and Notes

(1) Thomson, T. *Polyurethanes as Specialty Chemicals: Principles and Applications*; CRC Press: Boca Raton, 2005.
(2) Szycher, M. *Szycher's Handbook of Polyurethanes*; CRC Press: Boca Raton, 1999.
(3) Wirpsza, Z. *Polyurethanes: Chemistry, Technology and Application*; Harwood Publs.: New York, 1993.
(4) Hepburn, C. *Polyurethane Elastomers*, 2nd ed.: Elsevier Applied Science Publ.: London, 1991.
(5) Peppas, N. A.; Langer, R. *Science* **1994**, *263*, 1715.
(6) Koevoets, R. A.; Versteegen, R. M.; Kooijman, H.; Spek, A. L.; Sijbesma, R. P.; Meijer, E. W. *J. Am. Chem. Soc.* **2005**, *127*, 2999.
(7) Lendlein, A.; Langer, R. *Science* **2002**, *296*, 1673.
(8) Langer, R.; Tirrell, D. A. *Nature* **2004**, *428*, 487.
(9) Lendlein, A.; Jiang, H.; Junger, O.; Langer, R. *Nature* **2005**, *434*, 879.
(10) Wisse, E.; Spiering, A. J. H.; van Leeuwen, E. N. M.; Renken, R. A. E.; Dankers, P. Y. W.; Brouwer, L. A.; van Luyn, M. J. A.; Harmsen, M. C.; Sommerdijk, N. A. J. M.; Meijer, E. J. *Biomacromolecules* **2006**, *7*, 3385.
(11) Boretos, J. W.; Pierce, W. S. *Science* **1967**, *158*, 1481.
(12) Lee, B. S.; Chun, B. C.; Chung, Y. C.; Sul, K. I.; Cho, J. W. *Macromolecules* **2001**, *34*, 6431.
(13) Yilgor, E.; Yilgor, I.; Yurtsever, E. *Polymer* **2002**, *43*, 6551.
(14) Yilgor, E.; Yurtsever, E.; Yilgor, I. *Polymer* **2002**, *43*, 6561.
(15) Yeh, F.; Hsiao, B. S.; Sauer, B. B.; Michel, S.; Siesler, H. W. *Macromolecules* **2003**, *36*, 1940.
(16) Finnigan, B.; Jack, K.; Campbell, K.; Halley, P.; Truss, R.; Casey, P.; Cookson, D.; King, S.; Martin, D. *Macromolecules* **2005**, *38*, 7386.
(17) Miller, J. A.; Lin, S. B.; Hwang, K. K. S.; Wu, K. S.; Gibson, P. E.; Cooper, S. L. *Macromolecules* **1985**, *18*, 32.
(18) Lee, D.; Speckhard, T. A.; Sorensen, A. D.; Cooper, S. L. *Macromolecules* **1986**, *19*, 2383.
(19) Lee, D.; Register, R. A.; Yang, C.; Cooper, S. L. *Macromolecules* **1988**, *21*, 1005.
(20) Velankar, S.; Cooper, S. L. *Macromolecules* **1998**, *31*, 9181.
(21) Velankar, S.; Cooper, S. L. *Macromolecules* **2000**, *33*, 395.
(22) Koberstein, J. T.; Russell, T. P. *Macromolecules* **1986**, *19*, 714.
(23) Koberstein, J. T.; Galambos, A. F. *Macromolecules* **1992**, *25*, 5618.
(24) Leung, L. M.; Koberstein, J. T. *Macromolecules* **1986**, *19*, 706.
(25) Li, Y.; Gao, T.; Linliu, K.; Desper, C. R.; Chu, B. *Macromolecules* **1992**, *25*, 7365.
(26) Chen, T. K.; Shieh, T. S.; Chui, J. Y. *Macromolecules* **1998**, *31*, 1312.
(27) Klinedinst, D. B.; Yilgor, E.; Yilgor, I.; Beyer, F. L.; Wilkes, G. L. *Polymer* **2005**, *46*, 10191.
(28) Koerner, H.; Kelley, J. J.; Vaia, R. A. *Macromolecules* **2008**, *41*, 4709–4716.
(29) Hernandez, R.; Weksler, J.; Padsalgikar, A.; Choi, T.; Angelo, E.; Lin, J. S.; Xu, L. C.; Siedlecki, C. A.; Runt, J. *Macromolecules* **2008**, *41*, 9767.
(30) Shimura, Y.; Chen, D. *Macromolecules* **1993**, *26*, 5004.
(31) Boufi, S.; Belgacem, M. N.; Quillerou, J.; Gandini, A. *Macromolecules* **1993**, *26*, 6706.
(32) Wang, C. B.; Cooper, S. L. *Macromolecules* **1983**, *16*, 775.
(33) Nitzsche, S. A.; Hsu, S. L.; Hammond, P. T.; Rubner, M. F. *Macromolecules* **1992**, *25*, 2391.
(34) Mattia, J.; Painter, P. *Macromolecules* **2007**, *40*, 1546.
(35) Williams, S. R.; Wang, W.; Winey, K. I.; Long, T. E. *Macromolecules* **2008**, *41*, 9072.
(36) Zhang, J.; Hu, C. P. *Eur. Polym. J.* **2008**, *44*, 3708.
(37) Kojio, K.; Nakashima, S.; Furukawa, M. *Polymer* **2007**, *48*, 997.
(38) Maiti, P.; Radhakrishnan, D.; Aruna, P.; Ghosh, G. *Macromol. Symp.* **2006**, *241*, 51.
(39) McLean, R. S.; Sauer, B. B. *Macromolecules* **1997**, *30*, 8314.
(40) Nair, B. R.; Osbourne, A. R.; Hammond, P. T. *Macromolecules* **1998**, *31*, 8749.
(41) Lee, H. S.; Hsu, S. L. *Macromolecules* **1989**, *22*, 1100.
(42) Teo, L. S.; Chen, C. Y.; Kuo, J. F. *Macromolecules* **1997**, *30*, 1793.
(43) Lee, J. B.; Kato, T.; Yoshida, T.; Uryu, T. *Macromolecules* **1993**, *26*, 4989.
(44) Lee, D. J.; Lee, J. B.; Koide, N.; Akiyama, E.; Uryu, T. *Macromolecules* **1998**, *31*, 975.
(45) Nair, B. R.; Gregoriou, V. G.; Hammond, P. T. *Polymer* **2001**, *41*, 2961.

(46) Seymour, R. W.; Estes, G. M.; Cooper, S. L. *Macromolecules* **1970**, *3*, 579.
(47) Seymour, R. W.; Cooper, S. L. *Macromolecules* **1973**, *6*, 48.
(48) Koberstein, J. T.; Galambos, A. F.; Leung, L. M. *Macromolecules* **1992**, *25*, 6195.
(49) Rogulska, M.; Kultys, A.; Podkoscielny, W. *Eur. Polym. J.* **2007**, *43*, 1402.
(50) Li, Y.; Ren, Z.; Zhao, M.; Yang, H.; Chu, B. *Macromolecules* **1993**, *26*, 612.
(51) Desper, C. R.; Byrne, C. A.; Li, Y.; Chu, B. *Macromolecules* **1995**, *28*, 4213.
(52) Lee, H. S.; Yoo, S. R.; Seo, S. W. *J. Polym. Sci., Part B* **1999**, *37*, 3233.
(53) Miller, J. A.; Cooper, S. L.; Han, C. C.; Pruckmayr, G. *Macromolecules* **1984**, *17*, 1063.
(54) Mang, J. T.; Hjelm, R. P.; Orler, E. B.; Wrobleski, D. A. *Macromolecules* **2008**, *41*, 4358.
(55) Sun, Y. S.; Jeng, U. S.; Huang, Y. S.; Liang, K. S.; Lin, T. L.; Tsao, C. S. *Physica B* **2006**, *385*−*386*, 650.
(56) Kautz, H.; van Beek, D. J. M.; Sijbesma, R. P.; Meijer, E. W. *Macromolecules* **2006**, *39*, 4265.
(57) Sheth, J. P.; Wilkes, G. L.; Fornof, A. R.; Long, T. E.; Yilgor, I. *Macromolecules* **2005**, *38*, 5681.

JP100599U